

Article

Layered and Cubic Semiconductors $AGaM'Q_4$ ($A^+ = K^+, Rb^+, Cs^+, Tl^+$; $M'4^+ = Ge4^+, Sn4^+$; $Q2^- = S2^-, Se2^-$) and High Third-Harmonic Generation

Daniel Friedrich, Hye Ryung Byun, Shiqiang Hao, Shane Patel,
 Christopher Wolverton, Joon Ik Jang, and Mercouri G. Kanatzidis

J. Am. Chem. Soc., **Just Accepted Manuscript** • DOI: 10.1021/jacs.0c08638 • Publication Date (Web): 15 Sep 2020

Downloaded from pubs.acs.org on September 15, 2020

Just Accepted

“Just Accepted” manuscripts have been peer-reviewed and accepted for publication. They are posted online prior to technical editing, formatting for publication and author proofing. The American Chemical Society provides “Just Accepted” as a service to the research community to expedite the dissemination of scientific material as soon as possible after acceptance. “Just Accepted” manuscripts appear in full in PDF format accompanied by an HTML abstract. “Just Accepted” manuscripts have been fully peer reviewed, but should not be considered the official version of record. They are citable by the Digital Object Identifier (DOI®). “Just Accepted” is an optional service offered to authors. Therefore, the “Just Accepted” Web site may not include all articles that will be published in the journal. After a manuscript is technically edited and formatted, it will be removed from the “Just Accepted” Web site and published as an ASAP article. Note that technical editing may introduce minor changes to the manuscript text and/or graphics which could affect content, and all legal disclaimers and ethical guidelines that apply to the journal pertain. ACS cannot be held responsible for errors or consequences arising from the use of information contained in these “Just Accepted” manuscripts.

Layered and Cubic Semiconductors $AGaM'Q_4$ ($A^+ = K^+, Rb^+, Cs^+, Tl^+$; $M'^{4+} = Ge^{4+}, Sn^{4+}$; $Q^{2-} = S^{2-}, Se^{2-}$) and High Third-Harmonic Generation

Daniel Friedrich,^a Hye Ryung Byun,^c Shiqiang Hao,^b Shane Patel,^b Chris Wolverton,^b Joon Ik Jang,^c Mercuri G. Kanatzidis^{*,a}

^a Department of Chemistry, Northwestern University, Evanston, Illinois 60208, United States

^b Department of Materials Science and Engineering, Northwestern University, Evanston, Illinois 60208, United States

^c Department of Physics, Sogang University, 35 Baekbeom-ro, Mapo-gu, Seoul 04107, Korea

Chalcogenide semiconductors, polymorphism, nonlinear optics

ABSTRACT: Eighteen new quaternary chalcogenides $AGaM'Q_4$ ($A^+ = K^+, Rb^+, Cs^+, Tl^+$; $M'^{4+} = Ge^{4+}, Sn^{4+}$; $Q^{2-} = S^{2-}, Se^{2-}$) have been prepared by solid-state syntheses and structurally characterized using single-crystal X-ray diffraction techniques. These new phases crystallize in a variety of layered structure types. The tin analogues also adopt an extended three-dimensional network structure as polymorphs. The polymorphism and phase-stability in these cases were studied by thermal analysis and high-temperature *in situ* X-ray powder diffraction. All compounds are semiconductors with the colored selenides absorbing light in the infrared-green region ($1.8 \text{ eV} < E_g < 2.3 \text{ eV}$) and the mostly white sulfides absorbing light in the blue-ultraviolet range ($2.5 \text{ eV} < E_g < 3.6 \text{ eV}$). Based on third-harmonic generation (THG) measurements, the third-order nonlinear optical (NLO) susceptibilities $\chi^{(3)}$ of the new and previously reported $AGaM'Q_4$ compounds were determined. These measurements revealed an apparent correlation between the THG response of the sample and its band gap, rather than the crystal structure type. While low-gap materials possess higher nonlinearity in general, we found that layered orthorhombic $RbGaGeS_4$ exhibits an impressive $\chi^{(3)}$ value (about four times larger than that of $AgGaS_2$) even with a large band gap and shows stability under ambient conditions with no significant irradiation damage.

Introduction

Quaternary chalcogenide compounds $A_aM_bM'_cQ_d$ (A = alkali metal, thallium; M, M' = transition or main group metal; Q = chalcogen) are an interesting class of solids with a large variety of stoichiometric compositions and structures. Quaternary compounds $A_aM_bM'_cQ_d$ (A = alkali metal, thallium; M = group 13 metal; M' = group 14 metal; Q = chalcogen) promise to deliver broad sets of chemical and physical functions depending on their structure types and compositions. Examples include the fast ion exchange in $KInSn_2S_6$ ¹ for the capture of lanthanide ions and the strong nonlinear optical (NLO) second-harmonic generation (SHG) of noncentrosymmetric compounds. Materials like $LiGaGe_2Q_6$,²⁻⁵ $A_2In_2M'Q_6$,⁶⁻⁹ and $TlGaSn_2Q_6$ ¹⁰⁻¹³ are especially promising NLO candidates. For the compounds with the stoichiometric composition $AMM'Q_4$ ($A = K, Rb, Cs, Tl$; $M = Al, Ga, In$; $M' = Si, Ge, Sn$; $Q = S, Se$), compounds containing indium and mixtures of gallium and tin have been mostly reported.¹⁴⁻²² Among the respective gallium germanium compounds only

$KGaGeS_4$ has been reported.²⁰ The present work deals with the discovery, structural characterization, and optical properties of a series of new gallium compounds $AGaM'Q_4$ ($A = K, Rb, Cs, Tl$; $M' = Ge, Sn$; $Q = S, Se$). In the course of our work we successfully managed to prepare and structurally characterize new compositions in these systems. Furthermore, we also discovered new crystalline polymorphs. For the quaternary gallium chalcogenides, different dimensionalities of the crystal structures are observed. The lighter gallium germanium phases solely crystallize as layered compounds with varying symmetry and different polymorphs. $CsGaGeS_4$ for example crystallizes in three different two-dimensional (2D) layered structures. For the heavier gallium tin compounds, such two-dimensional structures are also observed. However, these phases appear to also be stable in a three-dimensional (3D) network structure depending on the syntheses conditions.

We characterized the optical properties of our new materials using UV/vis optical spectroscopy and first-principles quantum chemical density functional theory

(DFT) calculations. Our results revealed that all these compounds are semiconductors with the colored selenides absorbing light in the infrared (IR)-green region ($1.8 \text{ eV} < E_g < 2.3 \text{ eV}$) and the mostly white sulfides absorbing light in the blue-ultraviolet (UV) range ($2.5 \text{ eV} < E_g < 3.6 \text{ eV}$). As all isolated phases are centrosymmetric solids, they have no SHG properties. While studies of SHG in the context of the crystal structure has been of interest for many years, the study of third-harmonic generation (THG) is relatively rare in the literature and the corresponding database of such properties is small. Therefore, unlike the case with SHG materials, it is difficult to develop an intuitive understanding of structure/property relationships with response to THG. As a set, these iso-stoichiometric compounds present an opportunity to study the NLO properties in such a context. Since THG occurs in all materials regardless of their symmetry, we therefore investigated these compounds regarding their third-order NLO properties. Here, we measured THG and assessed the third-order nonlinearity $\chi^{(3)}$ of powdered samples.^{23, 24} We found that several title compounds possess large third-order susceptibilities that exceed the $\chi^{(3)}$ values of the reference materials, AgGaS₂ or AgGaSe₂. Furthermore, a trend of increasing nonlinearity with a decrease of the optical band gap is observed in the $AGaM'Q_4$ compounds, independent of the crystal structure. Intriguingly, however, we found that RbGaGeS₄ is an outlier, possessing a high THG response and a large band gap at the same time. Our results show that these compounds are promising for third-order NLO applications that rely on nonlinear refractive index and two-photon absorption.²⁵

Experimental section

Starting materials. Commercially available chemicals potassium (K, Sigma Aldrich, 99.95 %), rubidium (Rb, Alfa Aesar, 99.5 %), cesium (Cs, Alfa Aesar, 99.5 %), thallium (Tl, Alfa Aesar, 99.99 %) gallium (Ga, 5N MET, 99.99%), germanium (Ge, American Elements, 99.99 %), tin (Sn, American Elements, 99.99 %), sulfur (S, 5N Plus, 99.999 %), and selenium (Se, American Elements, 99.999 %) were used without further purification. The A_2Q ($A = K, Rb, Cs$; $Q = S, Se$) were prepared by reaction of the alkali metals with the respective chalcogens in liquid ammonia.²⁶ Gallium chalcogenides were prepared by reaction of Ga and the respective chalcogen at 1000 °C (Ga₂S₃) and 600 °C (Ga₂Se₃), respectively. GeS₂ and SnS₂ were prepared by annealing of the elements at 800 °C and 550 °C, respectively.

Synthesis of the title compounds. All quaternary compounds were prepared by high-temperature reaction of stoichiometric amounts of the respective starting materials in flame-sealed and evacuated fused silica

tubes. In a typical reaction batch of 1.0 g, stoichiometric amounts of alkali metal chalcogenides A_2Q combined with the other precursor materials were weighed in a fused silica tube (inner diameter 8mm) in a nitrogen-filled glovebox. The tubes were evacuated to $\sim 10^{-4}$ mbar and flame-sealed. The $\sim 10 - 11$ cm long tubes were placed in a programmable furnace and annealed according to the respective heating programs. The full details on the syntheses and temperature programs can be found in the Supplementary Information. After opening of the tubes, phase-purity and crystallinity of the resulting materials were determined by X-ray powder diffraction techniques. Unless otherwise noted, all samples are single-phase solids. X-ray powder diffraction patterns of all new phases that could be produced in larger bulk quantities are shown in the Supplementary Information (Figures S1-S4). A general rule for the synthesis of these $AGaM'Q_4$ compounds seems that the layered 2D polymorphs only form at high temperatures or after cooling of a molten batch, while the 3D network compounds need to be annealed for an extended amount of time below the melting point. All sulfide compounds are stable in moist air, while the selenides decompose within several minutes by releasing gaseous H₂Se and turning black. The samples were therefore stored in a glovebox and only exposed to air for minimal time before any characterization.

Single crystal X-ray diffraction. Suitable single crystals of the title compounds were selected under a microscope and fixed to MiTeGen mounts using silicon grease. Diffraction data was collected at ambient temperatures on a Bruker Kappa APEX II diffractometer equipped with an I μ S microfocus X-ray (Mo-K α radiation, $\lambda = 0.71073 \text{ \AA}$) source and an APEX2 CCD detector. The resulting diffraction data were corrected for Lorentz and polarization effects, and absorption was corrected by a numerical absorption correction (based on the crystal faces) using the Bruker APEX II software suite. All data sets had a completeness of 99.9 % within $50^\circ 2\theta$. The crystal structures were solved by intrinsic phasing methods using ShelXT2018/3 and refined on F^2 with ShelXL2018/3 using full-matrix least squares methods.

Further details on the crystal structure investigations may be obtained from the Fachinformationszentrum Karlsruhe, 76344 Eggenstein-Leopoldshafen, Germany (fax: (+49)7247-808-666; E-mail: crysdata@fiz-karlsruhe.de), on quoting the depository numbers CSD-2018860 for RbGaGeS₄ (**1**), CSD-2018859 for RbGaGeSe₄ (**2**), CSD-2018866 for TlGaGeS₄ (**3**), CSD-2018863 for TlGaGeSe₄-oP56 (**4**), CSD-2018857 for CsGaGeS₄-oP56 (**5**), CSD-2018862 for CsGaGeSe₄ (**6**), CSD-2018854 for CsGaSnS₄-oP56 (**7**), CSD-2018855 for KGaGeSe₄ (**8**), CSD-2018869 for TlGaSnS₄-mP56 (**9**), CSD-2018867 for TlGaSnSe₄-mP56 (**10**), CSD-2018861 for TlGaGeSe₄-

mC112 (**11**), CSD-2018853 for CsGaGeSe₄-*mP28* (**12**), CSD-2018852 for CsGaGeSe₄-*aP28* (**13**), CSD-2018856 for KGaSnSe₄-*cP84* (**14**), CSD-2018858 for RbGaSnSe₄-*cP84* (**15**), CSD-2018865 for TlGaSnSe₄-*cP84* (**16**), CSD-2018868 for TlGaSnSe₄-*cP84* (**17**), and CSD-2018864 for CsGaSnSe₄-*cP84* (**18**). All compounds presented in this work have mixed occupation of the Ga³⁺ and M⁴⁺ cations on all respective sites. For a charge balanced compound, the ideal ratio of Ga³⁺/M⁴⁺ in all compounds has to be 1:1. Therefore, all initial structure refinements were performed under the assumption of equal occupancy of Ga³⁺ and Ge⁴⁺ or Sn⁴⁺, respectively. For the layered mixed Ga³⁺/Sn⁴⁺ compounds, however, large low electron density maxima on the difference Fourier map and large *R* values were obtained after the initial refinement. In order to properly treat the mixed occupation, all metal occupation factors were freely refined. The resulting structure models converged in all cases with a total Ga³⁺/M⁴⁺ ratio of 1:1. As we wanted to treat the mixed Ga³⁺/Sn⁴⁺ occupation with the least amount of restrictions possible, the occupation factors in these structures were refined using free variables for all sites. All sites in the Ga³⁺/Ge⁴⁺ compounds were kept at 50% occupancy for both cations as they cannot be properly distinguished using conventional single-crystal X-ray techniques. For the alkali metal compounds, all refinements converged with a perfect 1:1 ratio of Ga³⁺ and Sn⁴⁺ and full occupancy of all A⁺ and Q²⁻ sites. Additional constraints in the form of a SUMP command were therefore not necessary. All layered thallium compounds show a severe disorder on all TI⁺ sites, which was treated by splitting the site in two new sites and free refinement of the occupation factors using another free variable to ensure charge balance. The structural refinement of the compound labeled TlGaGeSe₄-*mC112* revealed that this phase is in fact not an ideal *AMM'Q*₄ compound as its stoichiometry converged with the sum formula Tl_{0.8}Ga_{0.8}Ge_{1.2}Se₄ and one not fully occupied TI⁺ site. For this compound, the occupation factors of TI⁺, Ga³⁺, and Ge⁴⁺ were also constraint using a SUMP command.

X-ray powder diffraction. X-ray powder diffraction patterns were collected on a Rigaku Miniflex600 diffractometer using Cu-Kα1 radiation ($\lambda = 0.154593$ Å) equipped with a high-speed silicon strip detector. Finely powdered samples were measured on a flat zero-background Si sample. The experimental patterns were compared to simulated patterns based on the experimental CIF files.

In situ high-temperature X-ray powder diffraction. For the high-temperature X-ray diffraction experiments, powdered samples were flame-sealed in evacuated fused silica capillaries (diameter 0.3 mm). The samples were measured on a STOE Stadi P

diffractometer equipped with a Dectris Mythen 1K detector using monochromatic Mo-Kα1 radiation ($\lambda = 0.70930$ Å). The samples were heated by a STOE high-temperature capillary furnace. The WinX^{POW} software package from STOE & Cie was used for data collection and processing.

UV/Vis diffuse reflectance spectroscopy. The diffuse-reflectance measurements were performed at room temperature using a Shimadzu UV-3101 PC double-beam, double-monochromator spectrometer. BaSO₄ was used as a white standard (100 % reflectance) and spectra were collected in the range of 200 – 2500 nm with a resolution of 2 nm. The absorption spectra were calculated from the raw data using the Kubelka-Munk equation.²⁷

Differential thermal analysis. For the differential thermal analysis, powdered samples (~ 25 mg) were flame-sealed in fused silica ampoules. The measurements were performed on a Netzsch STA F3 Jupiter operating in thermogravimetric analysis-DTA mode. Two heating- and cooling cycles of all samples were collected with heating- and cooling rates of 10°C/min. A similarly prepared Al₂O₃ sample was used as a reference material.

Density Functional Theory (DFT) calculations. DFT calculations within the generalized gradient approximation (GGA) were used to calculate electronic structures of the title compounds. The Perdew-Burke-Ernzerhof exchange correlation functional with Projector Augmented Wave potentials were applied to all calculations.²⁸ The periodic boundary conditions and a plane-wave basis set were utilized as implemented in the Vienna ab initio simulation package.²⁹ The total energies were numerically converged to approximately 3 meV/cation using a basis set energy cutoff of 500 eV and dense *k*-meshes corresponding to 4000 *k*-points per reciprocal atom in the Brillouin zone. In order to find proper structure models for the mixed Ga³⁺/M⁴⁺ occupation, the lowest energy configuration was chosen from a vast number of geometrically distinct Ga³⁺/M⁴⁺ possibilities. For the 10 structures with the lowest electrostatic energies, further DFT calculations were performed to identify the most favorable (lowest energy) configuration.

Third-harmonic generation (THG) measurements. The phase-matching (PM) behavior of the title compounds was investigated using polycrystalline powdered samples. For each compound, six fractions of different grain sizes (25-32 μm, 32-45 μm, 45-62 μm, 62-90 μm, 90-106 μm, and 106-150 μm) were prepared by mechanical sieving of the finely grounded powders. Each sample was flame-sealed in a glass capillary (diameter 1 mm) to prevent moisture and air exposure, and mounted on a homemade sample holder. The THG efficiencies of

the samples with wide (narrow) bandgaps were compared with a reference material AgGaS₂ (AgGaSe₂).

The THG measurements were carried out at room temperature using input wavelengths of $\lambda = 1800$ nm and 2400 nm, respectively, for wide-gap and narrow-gap compounds with an intensity of 2.74 GW/cm². This intensity did not result in any significant irradiation damage. Coherent light with a wavelength of 1064 nm was initially produced using an EKSPLA PL-2250 series diode-pumped Nd:YAG laser with a pulse width of 30 ps and a repetition rate of 50 Hz to generate tunable pulses. The Nd:YAG laser pumped an EKSPLA Harmonics Unit (HU) H400, in which the input beam was frequency tripled by a sum frequency generation scheme. The beam then entered an EKSPLA PG403-SH-DFG Optical Parametric Oscillator (OPO) composed of four main parts: (i) a double-pass parametric generator, (ii) a single pass parametric amplifier, (iii) a second-harmonic generator (SH), and (iv) a difference frequency generation (DFG) scheme. The output wavelengths of the OPO used in our experiments were 1800 nm and 2400 nm. These wavelengths were deliberately selected in order to make sure that THG (600 nm and 800 nm) occurs below the bandgap of both test samples and reference materials. This implies that the effect of multiphoton absorption can be neglected in our measurements, and therefore, THG arises mostly from the real part of the third-order nonlinearity. The THG signal was collected using a reflection geometry and a fiber-optic bundle coupled to a spectrometer (Horiba iHR320) equipped with a CCD camera (Horiba Synapse). The data collection time was 450 s.

Results and discussion

Prior to this work, KGaGeS₄²⁰ and a series of AGaSnQ₄ (A = K, Rb, Tl, Cs; Q = S, Se)^{16, 17, 19, 20, 30} compounds were the only reported quaternary compounds with the stoichiometric composition AGaM'Q₄ (M' = Ge, Sn) in literature. In this work we successfully prepared all previously unknown combinations and in some cases discovered new crystalline polymorphs. As most quaternary compounds reported in this work crystallize in more than one crystalline modification or represent a new polymorph of an already known composition, in order to distinguish these polymorphs, we added the Pearson symbol (e.g. *-oP56*, *-mP56*, *-cP84*) at the end of the sum formula as a unique identifier as suggested by the IUPAC and IUCr. The symbols indicate the crystal system, lattice centering, and number of atoms per unit cell, respectively.

Crystal structure description. Due to the large amount of structures and structure types, only the most important aspects of the crystal structures of the new compounds will be discussed here. Further crystal

structure data and interatomic distances are listed in the Supplementary Information (Tables S1-S72).

The AGaM'Q₄ (A = K, Rb, Cs; M' = Ge, Sn; Q = S, Se) compounds form plate-shaped crystals and crystallize in 2D layered structures.^{14, 16-20, 22, 30, 31} The structure of the layers found in these compounds is related to the high-temperature modification of GeS₂ (in this work called GeS₂-*mP48*).³² In order to better understand the layered structures it is best to break them into different building units and to describe the layers as being composed of condensed corner-sharing tetrahedra chains linked by edge-sharing Ge₂S₆ double tetrahedra units perpendicular to the chain direction. Each Ge₂S₆ linker is connected to two consecutive tetrahedra in the chains by four common corners (Figure 1a). In GeS₂-*mP48*, the Ge⁴⁺ cations occupy four crystallographically independent atomic sites with two each located in the corner-sharing chain and the double tetrahedra. For reasons of consistency, the sites forming the M₂Q₆ linkers (M = Ga/Ge, Ga/Sn) are referred to as M1 and M2, and the sites of the corner-sharing tetrahedra chain are labeled M3 and M4 for all layered polymorphs in this work (site labels can be found in Figure 1). The only exception to this labeling scheme is monoclinic CsGaGeS₄-*mP28* which only has two M sites, thus making M2 the linker site.

The substitution of half of the Ge⁴⁺ cations with Ga³⁺ cations in these layers, creates anionic layers $\frac{2}{\infty}$ [GaGeS₄]. In order to preserve charge balance, alkali metal counter cations fill the voids in and between the anionic layers. The specific combination of the elements also influences the symmetry of the resulting structure with the higher symmetry orthorhombic polymorphs exhibiting the most regular layers, compared to the lower symmetry monoclinic and triclinic polymorphs. The crystal structures of the different layered AGaM'Q₄ polymorphs are discussed in more detail below.

The monoclinic polymorph CsGaGaS₄-*mP28* (**12**) crystallizes in the space group *P2₁/c* and is isotypic to the known compound KGaGeS₄.²⁰ The structure of this compound is closely related to GeS₂-*mP48* as it retains an identical connectivity of the atoms in the anionic layers. Furthermore, the unit cell parameters of the solid and its parent structure are very similar with GeS₂-*mP48* having an axis along the layers doubled and a different monoclinic angle. These differences likely result from the incorporation of the alkali metal cations A⁺ in between the anionic layers, causing a distortion in the structure. Consequently, the anionic layers in CsGaGaS₄-*mP28* have a slightly more distorted shape than GeS₂ layers due to the cations widening the gap between the layers.

A triclinic polymorph of CsGaGeS₄, CsGaGaS₄-*aP28* (**13**), crystallizes in the triclinic space group *P1* isotypic to the known compounds KGaSnS₄ and KInGeS₄.²⁰ The

anionic substructure of this phase retains the ${}^2_{\infty}[\text{GaGeSe}_4]$ layers found in $\text{CsGaGeSe}_4\text{-}mP28$ and $\text{GeS}_2\text{-}mP48$. The lower symmetry of the structure, however, results in a significant distortion of the layers giving them a “wavy” look (Figure 1) when viewed parallel to the layers. Interestingly, the Cs^+ cations in this phase are also nine-fold coordinated by the S^{2-} anions like in $\text{CsGaGeSe}_4\text{-}mP28$, and the mean distances $\bar{d}(\text{Ga}/\text{Ge}-\text{S})$ are basically identical. The main structural difference between $\text{CsGaGaSe}_4\text{-}oP28$ and its monoclinic polymorph is that in monoclinic $\text{CsGaGaSe}_4\text{-}mP28$, the anionic layers are completely separated by the Cs^+ cations, while in the triclinic structure the Cs^+ cations are closer to the layers.

Because of the increased symmetry (orthorhombic, space group $Pnma$) in the mixed Ga/Ge compounds RbGaGeSe_4 (**1**), RbGaGeSe_4 (**2**), TlGaGeSe_4 (**3**), $\text{TlGaGeSe}_4\text{-}oP56$ (**4**), CsGaGeSe_4 (**5**), $\text{CsGaGeSe}_4\text{-}oP56$ (**6**), and $\text{CsGaSnSe}_4\text{-}oP56$ (**7**), a slight change in the layered structure occurs. Basic crystallographic data for these compounds can be found in Table 1. The same structure was also reported for the analogous $AMM'Q_4$ compounds CsInGeQ_4 ($Q = \text{S}, \text{Se}$)^{14, 16} and CsGaSnSe_4 .¹⁹ At first glance, the ${}^2_{\infty}[\text{Ga}M'Q_4]$ layers in the ab plane in this structure appear identical to the monoclinic layers found in $\text{GeS}_2\text{-}mP48$ and related compounds. The main difference of these layers to the $\text{GeS}_2\text{-}mP48$ type layers is the arrangement of the M_2Q_6 linkers, which are staggered in the $\text{GeS}_2\text{-}mP48$ type layers and aligned perfectly straight along the crystallographic a axis in the orthorhombic structures. Ga^{3+} and M^{4+} cations occupy only three crystallographically independent sites compared to the four in GeS_2 with $\text{Ga}/M1$ and $\text{Ga}/M2$ on special sites forming the Ga_2Q_6 linkers and the $\text{Ga}/M3$ site solely forming the linear chains (site labels see Figure 1). The higher symmetry sites lead to an overall less distorted appearance of the anionic layers compared to monoclinic GeS_2 . The A^+ cations ($A = \text{Rb}, \text{Cs}, \text{Tl}$) found in the voids in-between the anionic layers occupy two crystallographically independent sites. Both sites are nine-fold (7+2) coordinated by the chalcogenide anions within a sphere of 4.2 Å.

The compounds KGaGeSe_4 (**8**), $\text{TlGaSnSe}_4\text{-}mP56$ (**9**), and $\text{TlGaSnSe}_4\text{-}mP56$ (**10**), and the previously reported compounds KGaSnSe_4 ,¹⁹ $\text{RbGaSnSe}_4\text{-}mP56$,¹⁹ $\text{RbGaSnSe}_4\text{-}mP56$,³⁰ and KInSnSe_4 ¹⁸ crystallize in a 2D layered structure in the monoclinic space group $P2_1/c$. Basic crystallographic data for these compounds can be found in Table 2. This structure type, however, differs from $\text{GeS}_2\text{-}mP48$ layers in the same way as the orthorhombic layers by the arrangement of the M_2Q_6 linkers in the layers. This structure is basically a lower symmetry version of the orthorhombic $AMM'Q_4\text{-}oP56$ compounds

with the Ga^{3+} and M^{4+} cations occupying four crystallographically independent common sites. Consequently, the layers exhibit a slight distortion compared to the orthorhombic polymorphs.

In the batch of $\text{TlGaGeSe}_4\text{-}oP56$, a few single crystals of a different, monoclinic C-centered phase could be isolated. A free refinement of the crystal structure immediately revealed that the sum formula for this phase is “ $\text{Tl}_{0.8}\text{Ga}_{0.8}\text{Ge}_{1.2}\text{Se}_4$ ” (**11**). As the crystal structure is still related to the other phases and in order to distinguish this phase from orthorhombic $\text{TlGaGeSe}_4\text{-}oP56$, it will be labeled “ $\text{TlGaGeSe}_4\text{-}mC112$ ”. The anionic layers ${}^2_{\infty}[\text{GaGeSe}_4]$ in this compound run parallel to the (101) direction and have a slight distortion similar to the other monoclinic phases like $\text{TlGaSnQ}_4\text{-}mP56$ (Figure 1). All interatomic distances in both TlGaGeSe_4 polymorphs are basically identical. Both Tl^+ sites in $\text{TlGaGeSe}_4\text{-}mC112$ are nine-fold coordinated by Se^{2-} within 4.0 Å.

For all layered polymorphs of the $AGaM'Q_4$ compounds and related phases, the observed mean distances $\bar{d}(\text{Ga}/M'-Q)$ are basically identical for a given combination of elements with values of $\bar{d}(\text{Ga}/\text{Ge}-\text{S}) \approx 2.24(1)$ Å, $\bar{d}(\text{Ga}/\text{Sn}-\text{S}) \approx 2.34(1)$ Å, $\bar{d}(\text{Ga}/\text{Ge}-\text{Se}) \approx 2.38(1)$ Å, and $\bar{d}(\text{Ga}/\text{Sn}-\text{Se}) \approx 2.46(1)$ Å. Very minor variances can be attributed to slight influence of different A^+ cations. These values are also in good agreement with the sum of the ionic radii $d(\text{Ga}-\text{S}) = 2.31$ Å, $d(\text{Ge}-\text{S}) = 2.23$ Å, $d(\text{Sn}-\text{S}) = 2.39$ Å, $d(\text{Ga}-\text{Se}) = 2.45$ Å, $d(\text{Ge}-\text{Se}) = 2.37$ Å, and $d(\text{Sn}-\text{Se}) = 2.53$ Å.³³ The distances $d(\text{Ga}/M'-Q)$ in the $\text{Ga}/M'Q_4$ tetrahedra vary with the connectivity of the tetrahedra amongst each other. In the edge-sharing $(\text{Ga}/M')_2Q_6$ linker, the distances $d(\text{Ga}/M'-Q)$ are slightly shorter due to the edge-sharing and each tetrahedron only being connected to three adjacent tetrahedra. The distances $d(\text{Ga}/M'-Q)$ observed in the corner-sharing tetrahedra which are linked to four neighbors are slightly longer. Consequently, the distances $d(\text{Ga}/M'-\text{Ga}/M')$ in these tetrahedra also vary with the connectivity of the tetrahedra and shorter distances $d(\text{Ga}/M'-\text{Ga}/M')$ are observed in the edge-sharing linkers. In all layered polymorphs, all A^+ cation sites are nine-fold coordinated by Q^{2-} anions within a sphere of ~ 4.2 Å. The resulting polyhedra cannot be attributed to a regular coordination polyhedron. In the monoclinic polymorphs $AGaM'Q_4\text{-}mP56$, this nine-fold coordination is more akin to a 7+2 fold coordination with seven shorter distances $d(A-Q) < 4$ Å and two slightly longer distances $4 \text{ Å} < d(A-Q) < 4.2$ Å. All the observed distances in these compounds are in good agreement with already known $AMM'Q_4$ compounds^{20, 22, 31} and binary and ternary gallium,³⁴⁻⁵² germanium,^{32, 53-58} and tin⁵⁹⁻⁶⁷ compounds, respectively.

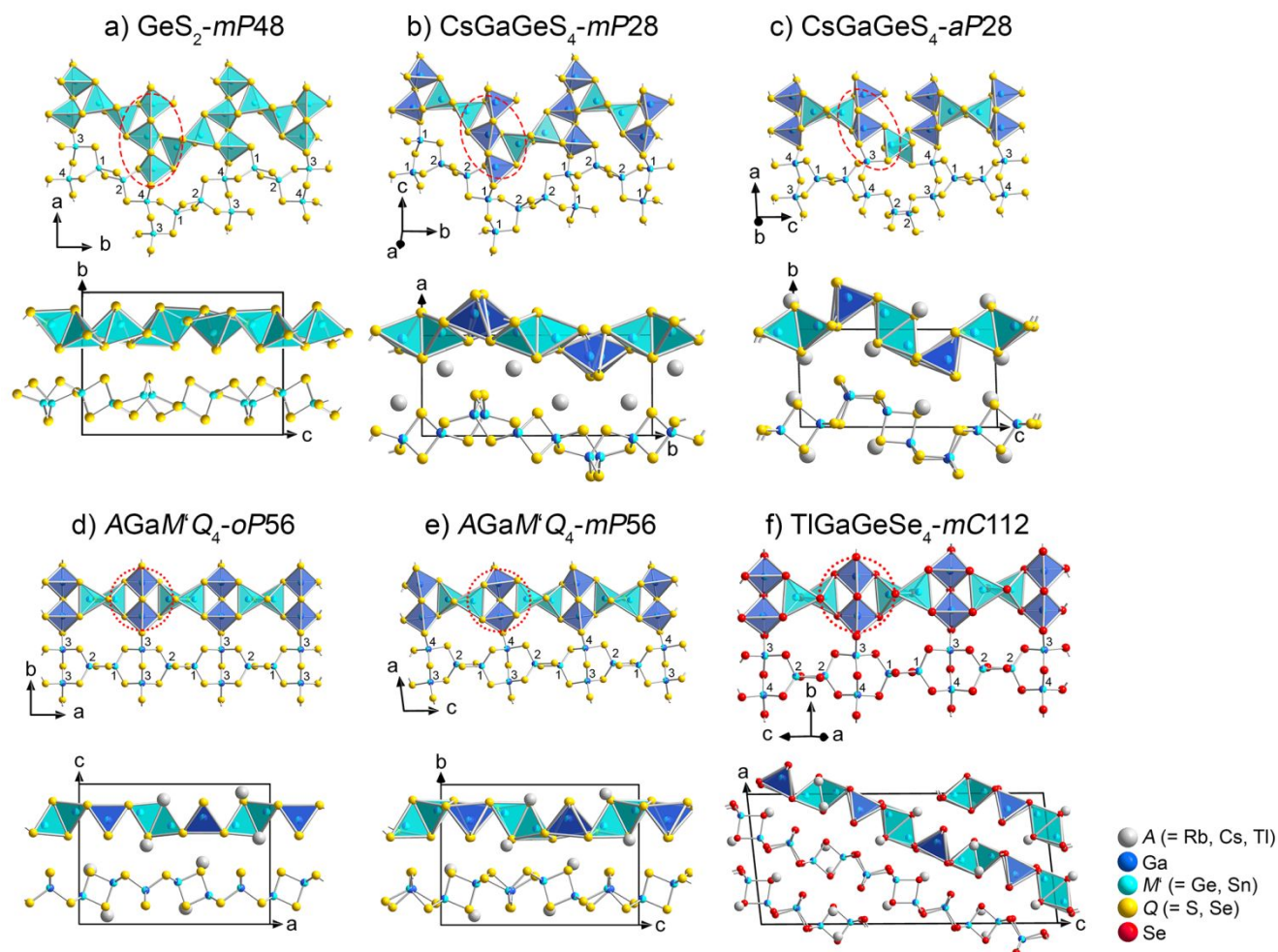


Figure 1. Crystal structures and sections of the anionic substructures of the layered $AGaM'Q_4$ phases (b-f) and their related structure GeS_2 - $mP48$ (a). The mixed Ga/ M' cation sites are labelled and the difference in the linkage of the atoms in the layers is highlighted by the dashed and dotted red circles, respectively.

Table 1. Crystallographic data* of the orthorhombic layered $AGaM'Q_4$ compounds.

	RbGaGeS ₄ (1)	RbGaGeSe ₄ (2)	TlGaGeS ₄ (3)	TlGaGeSe ₄ - <i>oP56</i> (4)	CsGaGeS ₄ - <i>oP56</i> (5)	CsGaGeSe ₄ (6)	CsGaSnS ₄ - <i>oP56</i> (7)
Space group	– <i>Pnma</i> (No. 60) –						
<i>a</i> /Å	16.8539(6)	17.5750(5)	16.7942(5)	17.4742(4)	17.0125(8)	17.7666(7)	17.5708(5)
<i>b</i> /Å	7.1330(3)	7.4718(2)	7.1027(2)	7.4105(2)	7.1848(3)	7.5171(3)	7.3846(2)
<i>c</i> /Å	12.1410(5)	12.4449(4)	11.5193(4)	11.9406(3)	12.5038(6)	12.6383(5)	12.4343(3)
<i>V</i> /Å ³	1459.6(1)	1634.2(1)	1374.07(7)	1546.2(1)	1528.4(1)	1687.9(1)	1613.4(1)
<i>Z</i>	– 8 –						
ρ_{calc} /g·cm ⁻³	3.240	4.419	4.564	5.692	3.507	4.652	3.699
$\mu(\text{Mo-K}\alpha)$ /mm ⁻¹	15.461	30.605	32.404	46.834	13.132	28.154	11.812
<i>T</i> /°C	– 20 –						
<i>R</i> _{int} , <i>R</i> _σ	0.0620, 0.0182	0.0465, 0.0136	0.0415, 0.0209	0.0482, 0.0231	0.0513, 0.0157	0.0562, 0.0184	0.0303, 0.0569
<i>R</i> ₁ , <i>wR</i> ₂ [<i>I</i> > 3σ(<i>I</i>)]	0.0206, 0.0499	0.0139, 0.0282	0.0199, 0.0383	0.0238, 0.0579	0.0154, 0.0306	0.0152, 0.0344	0.0191, 0.0447
<i>R</i> ₁ , <i>wR</i> ₂ [all data]	0.0258, 0.0519	0.0187, 0.0292	0.0270, 0.0406	0.0294, 0.0604	0.0190, 0.0316	0.0168, 0.0348	0.0209, 0.0460
$\Delta\rho_{\text{min}}$, $\Delta\rho_{\text{max}}$ /e·Å ⁻³	-0.537, 0.622	-0.503, 0.571	-1.154, 1.314	-1.671, 1.768	-0.509, 0.709	-0.680, 0.552	-0.762, 0.849

* The full details of the data collection and structural refinement can be found in the Supplementary Information.

Table 2. Crystallographic data* of the monoclinic and triclinic layered $AGaM'Q_4$ compounds.

	KGaGeSe ₄ (8)	TlGaSnS ₄ - <i>mP56</i> (9)	TlGaSnSe ₄ - <i>mP56</i> (10)	TlGaGeSe ₄ - <i>mC112</i> (11)	CsGaGeS ₄ - <i>mP28</i> (12)	CsGaGeS ₄ - <i>aP28</i> (13)
Space group	– <i>P2</i> ₁ / <i>c</i> –			<i>C2</i> / <i>c</i>	<i>P2</i> ₁ / <i>c</i>	<i>P</i> $\bar{1}$

$a / \text{\AA}$	7.3552(2)	7.2516(2)	7.501(1)	13.5831(4)	7.6995(5)	7.1611(1)
$b / \text{\AA}$	12.4151(3)	11.6629(4)	12.175(1)	7.4015(2)	16.3721(9)	7.5944(2)
$c / \text{\AA}$	17.6213(4)	17.5044(5)	18.203(1)	30.7410(7)	6.8930(4)	14.6345(3)
$\alpha / ^\circ$	90	90	90	90	90	91.003(2)
$\beta / ^\circ$	97.026(2)	95.267(3)	97.164(3)	96.066(2)	111.894(4)	92.314(2)
$\gamma / ^\circ$	90	90	90	90	90	106.680(2)
$V / \text{\AA}^3$	1597.02(7)	1474.18(8)	1649.4(2)	3073.3(1)	806.24(9)	761.42(3)
Z	- 8 -			16	4	4
$\rho_{\text{calc}} / \text{g}\cdot\text{cm}^{-3}$	4.136	4.695	5.646	5.379	3.324	3.520
$\mu(\text{Mo-K}\alpha) / \text{mm}^{-1}$	25.783	29.813	42.329	43.032	12.447	13.180
$T / ^\circ\text{C}$	- 20 -					
R_{int}, R_σ	0.0534, 0.0407	0.0503, 0.0311	0.0442, 0.0253	0.0446, 0.0265	0.0528, 0.0239	0.0393, 0.0222
$R_1, wR_2 [I > 3\sigma(I)]$	0.0257, 0.0458	0.0458, 0.1148	0.0358, 0.0853	0.0293, 0.0689	0.0231, 0.0572	0.0170, 0.0414
$R_1, wR_2 [\text{all data}]$	0.0439, 0.0499	0.0523, 0.1178	0.0434, 0.0887	0.0328, 0.0700	0.0277, 0.0603	0.0182, 0.0419
$\Delta\rho_{\text{min}}, \Delta\rho_{\text{max}} / \text{e}\cdot\text{\AA}^{-3}$	-0.662, 0.669	-1.710, 1.961	-1.758, 2.642	-1.243, 1.186	-1.259, 0.910	-0.631, 0.799

* The full details of the data collection and structural refinement can be found in the Supplementary Information.

Table 3. Crystallographic data* of the cubic network $\text{AGaM}'\text{Q}_4\text{-cP84}$ compounds.

	$\text{KGaSnSe}_4\text{-cP84}$ (14)	$\text{RbGaSnSe}_4\text{-cP84}$ (15)	$\text{TlGaSnS}_4\text{-cP84}$ (16)	$\text{TlGaSnSe}_4\text{-cP84}$ (17)	$\text{CsGaSnS}_4\text{-cP84}$ (18)
Space group	- $P\bar{a}3$ -				
$a / \text{\AA}$	13.5555(3)	13.7200(1)	12.9938(4)	13.4755(2)	13.379(1)
$V / \text{\AA}^3$	2490.8(2)	2582.6(1)	2193.9(2)	2447.0(1)	2391.0(1)
Z	- 12 -				
$\rho_{\text{calc}} / \text{g}\cdot\text{cm}^{-3}$	4.347	4.550	4.732	5.770	3.747
$\mu(\text{Mo-K}\alpha) / \text{mm}^{-1}$	24.185	28.459	30.050	43.768	11.954
$T / ^\circ\text{C}$	- 20 -				
R_{int}, R_σ	0.0505, 0.0236	0.0459, 0.0118	0.0561, 0.0335	0.0590, 0.0277	0.0500, 0.0087
$R_1, wR_2 [I > 3\sigma(I)]$	0.0188, 0.0349	0.0123, 0.0248	0.0201, 0.0421	0.0248, 0.0567	0.0103, 0.0229
$R_1, wR_2 [\text{all data}]$	0.0290, 0.0374	0.0155, 0.0254	0.0251, 0.0444	0.0273, 0.0583	0.0104, 0.0229
$\Delta\rho_{\text{min}}, \Delta\rho_{\text{max}} / \text{e}\cdot\text{\AA}^{-3}$	-0.522, 0.416	-0.313, 0.444	-0.486, 0.627	-0.976, 1.938	-0.433, 0.514

* The full details of the data collection and structural refinement can be found in the Supplementary Information.

For the mixed Ga/Sn phases $\text{KGaSnSe}_4\text{-cP84}$ (**14**), $\text{RbGaSnSe}_4\text{-cP84}$ (**15**), $\text{TlGaSnS}_4\text{-cP84}$ (**16**), $\text{TlGaSnSe}_4\text{-cP84}$ (**17**), and $\text{CsGaSnS}_4\text{-cP84}$ (**18**), polymorphs crystallizing in an entirely different 3D network structure were also found. Basic crystallographic data for these compounds can be found in Table 3. The full details of the data collection and structure refinement can be found in the supplementary material (Tables S1-S72). Known compounds from literature like the series of sulfide materials AGaSnS_4 ($A = \text{Na, K, Rb}$),¹⁷ $\text{AlInM}'\text{S}_4$ ($A = \text{Rb, Cs, Tl}$; $M' = \text{Ge, Sn}$),¹⁴ and cubic KInSnSe_4 ($\gamma\text{-KInSnSe}_4$)¹⁸ crystallize isotypic to these new phases. These network structures crystallize in the cubic space group $P\bar{a}3$ with a unit cell parameter of $a \approx 13 \text{ \AA}$ and are isotypic to the ternary phase BaGa_2S_4 .³⁹ However, as half of the Ga^{3+} cations are replaced by M'^{4+} ($M' = \text{Ge, Sn}$) cations, only monovalent A^+ cations allow for charge balanced structures. For a better description, the 3D network structure can be regarded as stacked layers connected by common chalcogenide anions. Figure 2a shows one such layer in the bc plane with atoms the in

the a direction ranging from $0 < x < 0.5$. Note that these directions can be exchanged accordingly as the structure crystallizes in a cubic space group. One such layer is composed of corner-sharing $(\text{Ga}/M')_3\text{Q}_9$ tetrahedra triplets that are linked to four other building blocks by common corners. Connection between the layers is achieved by condensation of the two unconnected corners of a $(\text{Ga}/M')_3\text{Q}_9$ unit each linking to one adjacent layer, thus resulting in the ${}^3[\text{GaM}'\text{Q}_4]$ network (Figure 2b). The A^+ counter cations are located in the cavities of the network on two crystallographically independent sites. The coordination of these A^+ cations drastically differs with the higher symmetry $4a$ site having an only slightly distorted cuboctahedral environment of 12 Q^{2-} anions ($\text{Q} = \text{S, Se}$) with distances $d(\text{A-Q})$ in the range from 3.75 \AA to 3.95 \AA . The lower symmetry $8c$ site is in a distorted octahedral coordination with significantly smaller distances $d(\text{A-Q})$ ranging from 3.30 - 3.65 \AA . Within a sphere of 4.0 \AA for the sulfides and 4.2 \AA for the selenides, respectively, three additional chalcogenide anions are located. For the thallium compounds, an

identical arrangement of the atoms is observed, however, the symmetry of the A^+ cation on the $4a$ site (0, 0, 0) is reduced. This symmetry reduction is most likely caused by the Tl^+ lone pair that is not present for the alkali metal cations. The softer selenide network seems to be able to compensate this lone-pair effect to a certain degree with the Tl^+ cation still occupying a special $8c$ site (0.02, 0.02, 0.02) in $TlGaSnSe_4$ -*cP84*. In the sulfide compound $TlGaSnS_4$ -*cP84*, however, this Tl^+ occupies a common $24c$ site (0.00, 0.02, 0.03).

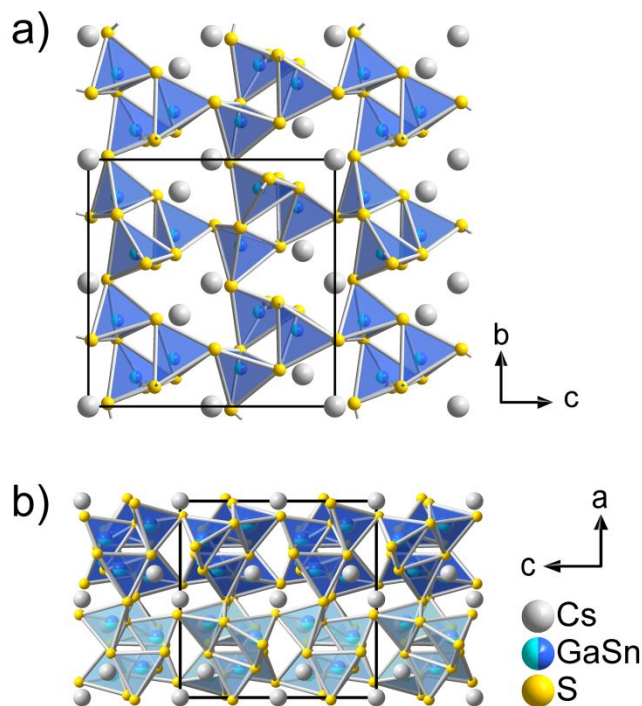


Figure 2. The crystal structure of the cubic network structure showing: a) A section of the corner-sharing layers in the bc plane used for the description of the structure; b) The extended network structure when viewed along (010) with two individual layers highlighted by different shades of blue.

Mixed site-occupation of M^{3+}/M^{4+} . One problem during the refinement of the crystal structures of the new $AGaGeQ_4$ phases was the distribution of the Ga^{3+} and M^{4+} cations in the structures. As it is not possible to distinguish Ga^{3+} and Ge^{4+} using conventional X-ray diffraction techniques, we decided to keep the Ga^{3+}/Ge^{4+} ratio fixed at 1:1 for these phases. The same, however, does not apply to the new mixed Ga^{3+}/Sn^{4+} phases $CsGaSnS_4$ -*oP56*, $TlGaSnQ_4$ -*mP56*, and the other Ga^{3+}/Sn^{4+} and In^{3+}/Ge^{4+} phases known from literature.^{14, 16, 19, 30} The results of the crystal structure refinements of our new and known Ga^{3+}/Sn^{4+} and In^{3+}/Ge^{4+} phases revealed that M^{3+} and M^{4+} cations are not evenly distributed but preferably occupy specific sites. On average about 65-70 % of the M^{4+} cations are located in the edge-sharing double tetrahedra linker and consequently 65-70 % of the M^{3+} cations are located in

the corner-sharing chains within the layers. As the same situation is observed for all phases, regardless of the size of the individual cations, this seems to be an intrinsic phenomenon of these Ga^{3+}/Sn^{4+} compounds and might result from the size difference of these cations. In $Tl_{0.8}Ga_{0.8}Ge_{1.2}Se_4$ ($TlGaGeSe_4$ -*mC112*) the same still applies, however, the additional Ge^{4+} cations are located in the corner-sharing tetrahedra chains resulting in a more even ratio of about 55 % Ge^{4+} and 45 % Ga^{3+} . As the cubic network polymorphs have only one M^{3+}/M^{4+} site and all other sites freely refine to full occupation, a ratio of 50:50 has to be assumed.

Polymorphism. Among the $AGaM'Q_4$ compounds, several compositions crystallize in more than one crystalline phase. Such cases include compounds crystallizing in the layered orthorhombic structure $AGaM'Q_4$ -*oP56* and the cubic network structure $AGaM'Q_4$ -*cP84*. This polymorphism has already been observed in similar compounds like $KInSnSe_4$ ¹⁸ and $CsInGeS_4$.¹⁴ For the composition $CsGaSnS_4$, the cubic polymorph was assumed, but no structural data was reported.¹⁷ In this work we managed to not only successfully grow crystals and provide data for the cubic phase $CsGaSnS_4$ -*cP84* (**17**), but also isolate and characterize the orthorhombic modification $CsGaSnS_4$ -*oP56* (**7**). Similarly, for the previously reported $KGaSnSe_4$,¹⁹ the new cubic polymorph $KGaSnSe_4$ -*cP84* (**14**) was assumed to exist, but could not be isolated or characterized. Based on our and the reported observations, we conclude this polymorphism can exist as a kinetic phase and a thermodynamic phase during the synthesis. For all listed cases we could reproducibly prepare the cubic polymorphs by (long-term) annealing of the reaction mixtures below the melting point of the phase, while the orthorhombic phases were always formed upon melting of the material and subsequent (slow) cooling. From these observations we conclude that the 3D cubic structure is the thermodynamic phase and the orthorhombic 2D structure is the kinetic phase. A similar situation was also observed for the compounds $TlGaSnQ_4$ (**9**, **10**, **16**, **17**), which crystallize in the cubic $AGaM'Q_4$ -*cP84* as well as the layered monoclinic $AGaM'Q_4$ -*mP56* polymorphs. Like the case discussed above, the cubic network phase $TlGaSnQ_4$ -*cP84* (**16**, **17**) can also reproducibly be prepared by annealing below the melting point. The layered monoclinic phase $TlGaSnQ_4$ -*mP56* (**9**, **10**) was obtained after (slow) cooling of the molten sample. These results and our investigations also lead to the assumption that the 3D cubic polymorph can only be realized for $AGaSnQ_4$ compounds and not for $AGaGeQ_4$ compounds, indicating some influence of the size and reactivity of the metal cations on the resulting structures.

In the case of CsGaGeS_4 , a more complex situation of three different layered polymorphs is observed. Upon the irreproducible discovery of triclinic CsGaGeS_4 -*aP28* (**13**), the thermal behavior of the polymorph was investigated using differential thermal analysis (DTA). This measurement, however, revealed no additional thermal events aside from the melting point at $\sim 840^\circ\text{C}$. An X-ray powder diffraction analysis following the measurement revealed that the sample had transformed to CsGaGeS_4 -*oP56* (**5**). In order to better understand this transformation, triclinic CsGaGeS_4 -*aP28* was investigated using *in situ* high-temperature X-ray powder diffraction (Figure 3). This analysis revealed that above 300°C the formation of a different phase was observed which remained until melting of the sample at $\sim 840^\circ\text{C}$. This new phase was identified as the monoclinic phase CsGaGeS_4 -*mP28* (**12**). After recrystallization of the melt at $\sim 800^\circ\text{C}$, only the orthorhombic phase CsGaGeS_4 -*oP56* (**5**) remained stable down to room temperature.

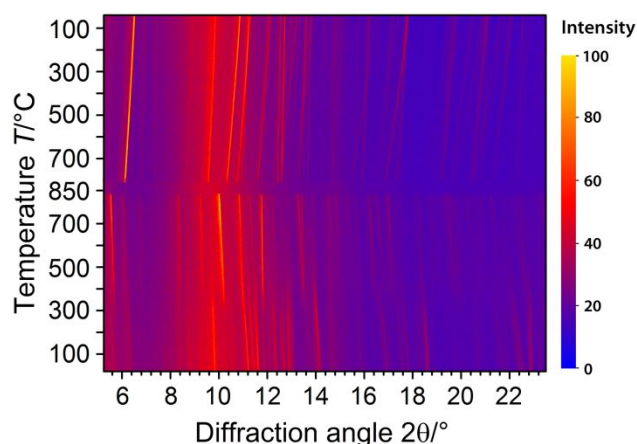


Figure 3. 2D plot of the *in situ* X-ray powder diffraction patterns of CsGaGeS_4 -*aP28* during one heating and cooling cycles in the temperature region of $25 - 850^\circ\text{C}$ (Mo- $\text{K}\alpha_1$ radiation).

CsGaGeS_4 -*aP28* could not be recovered by quenching of CsGaGeS_4 -*mP28* and subsequent annealing below the transition temperature, indicating an irreversible phase transition. The absence of orthorhombic CsGaGeS_4 -*oP56* during the initial heating phase likely results from the differences in connectivity in the ${}_{\infty}[\text{GaGeS}_4]$ layers. While CsGaGeS_4 -*aP28* and CsGaGeS_4 -*mP28* can be transformed by simple deformation of the structure, CsGaGeS_4 -*oP56* can only be formed by breaking and reforming chemical bonds. As only a small quantity of triclinic CsGaGeS_4 -*aP28* was prepared, no further investigations regarding these phases were performed. An overview of all the currently known $\text{AGaM}'\text{Q}_4$ phases ($A = \text{K, Rb, Cs, TI}$; $M' = \text{Ge, Sn}$; $Q = \text{S, Se}$) including all different polymorphs is shown in Figure 4.

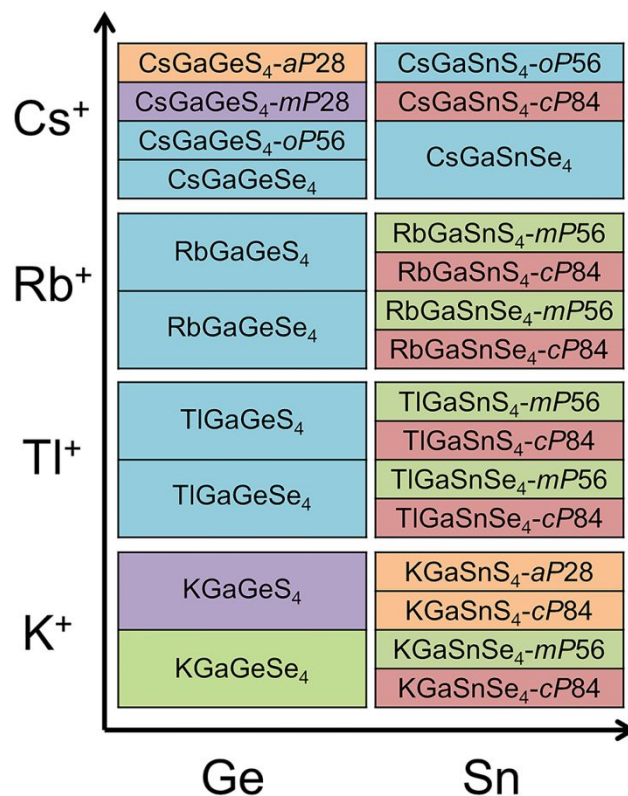


Figure 4. All currently known $\text{AGaM}'\text{Q}_4$ polymorphs ($A = \text{K, Rb, Cs, TI}$; $M' = \text{Ge, Sn}$; $Q = \text{S, Se}$) sorted by M' and the alkali metal cations A^+ . The different polymorphs are represented by the colored backgrounds: $\text{AGaM}'\text{Q}_4$ -*oP56* (blue), $\text{AGaM}'\text{Q}_4$ -*cP84* (red), $\text{AGaM}'\text{Q}_4$ -*mP56* (green), $\text{AGaM}'\text{Q}_4$ -*aP28* (orange), and $\text{AGaM}'\text{Q}_4$ -*mP28* (purple).

Optical properties. The optical absorption data are shown in Figure 5. The optical band gaps (E_g) were determined by extrapolation of the linear part of the absorption edge on the baseline. A clear trend of significantly smaller band gaps of the selenides with values $1.8\text{ eV} < E_g < 2.3\text{ eV}$ in the IR-green region can be observed. The sulfides are all wide-gap semiconductors with band gap values $2.5\text{ eV} < E_g < 3.6\text{ eV}$ in the blue-UV region.

For a given structure type and element composition, only marginal differences in the band gap values are observed for different alkali metal A^+ cations. Compounds like AGaGeS_4 -*oP56*, AGaGeSe_4 -*oP56*, and AGaSnS_4 -*cP84* ($A = \text{Rb, Cs}$), respectively, have basically identical band gap values for a given structure. This is consistent with the fact that the alkali metal states do not contribute to the states close to the Fermi level. Varying the M' cation in a given structure only results in slightly smaller band gaps. When substituting Ge^{4+} with Sn^{4+} in the orthorhombic layered structure, CsGaSnS_4 -*oP56* ($E_g = 3.07\text{ eV}$) only has a slightly smaller optical band gap than CsGaGeS_4 ($E_g = 3.18\text{ eV}$). A redshift of the band gaps is observed in the $\text{TlGaM}'\text{S}_4$ compounds

having a pale yellow color compared to the white $AGaM'S_4$ ($A = K, Rb, Cs$) powdered samples. This arises likely from the band gaps shrinking due to the electronic states contributed by the Tl^+ lone pair and empty p states. Among the thallium selenides, this effect is not very pronounced.

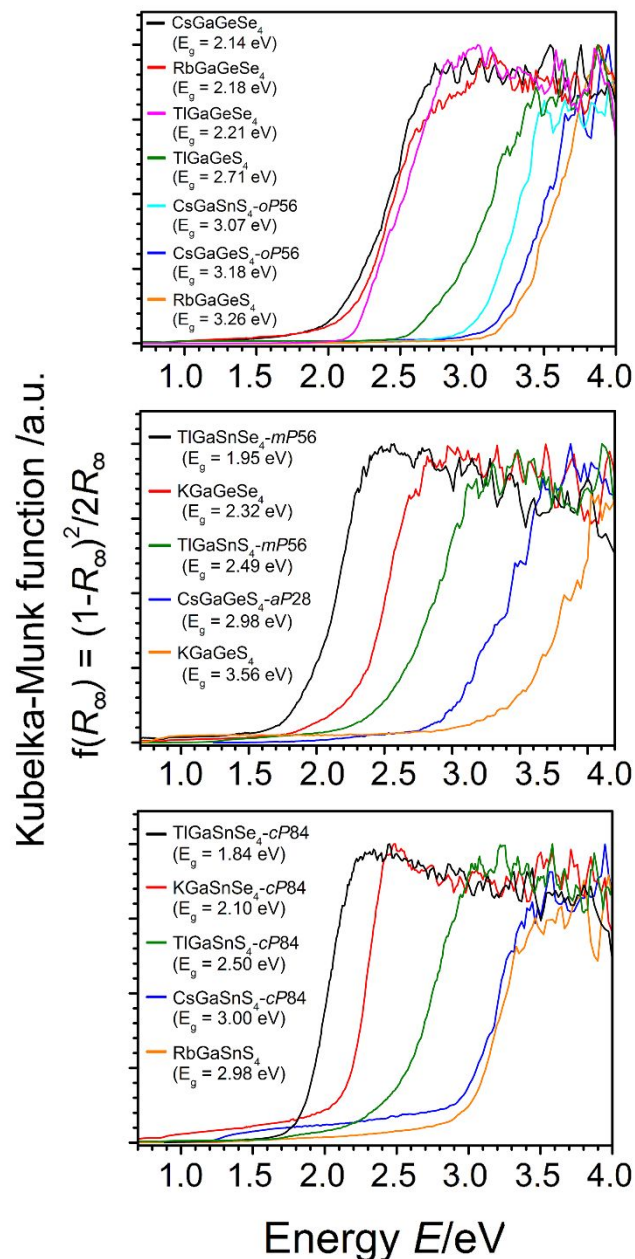


Figure 5. UV/Vis absorption spectra of orthorhombic layered compounds $AGaM'Q_4-oP56$ (top), monoclinic and triclinic layered compounds $AGaM'Q_4-aP28/-mP56$ (middle), and the 3D network structures $AGaM'Q_4-cP84$ (bottom). The values of the determined band gaps are given in the respective legends.

Complementary DFT calculations of the $AGaM'Q_4$ compounds (Figures S5-S19) were performed to give further insight in the electronic structure of these solids. Due to the vast amount of different polymorphs for most

element combinations, only one band structure and DOS was calculated for each combination. The calculations revealed that all quaternary chalcogenides are semiconductors with the states below the Fermi level being dominated by the $S-3p$, $Se-4p$, and $Ga-4p$ states, while the lowest states in the conduction bands are mostly $Ge-4s$, $Sn-5s$, and $Ga-3s$. In case of the thallium compounds, the $Tl-6s$ are also located at the Fermi level.

The type of band gap (direct or indirect) does not appear to be consistent for a certain structure type and changes with the combination of elements involved. Figure 6 shows band structure plots, representing the most prominent structures. Additional band structure plots and the respective density of states (DOS) plots can be found in the Supplementary Information (Figures S5-S19). In case of the 3D cubic structures $AGaSnQ_4-cP84$, all selenides have an indirect band gap, while the sulfides have a direct band gap. For the 2D layered polymorphs, all $AGaM'Q_4-oP56$, $AGaGeS_4-mP28$, and $AGaGeS_4-aP28$ compounds have a direct band gap.

The monoclinic 2D polymorphs $AGaSnQ_4-mP56$ and $KGaGeSe_4$ have a direct band gap. These trends are not always observed for the thallium compounds. Both $TlGaSnS_4-mP56$ and $TlGaSnSe_4-mP56$ have an indirect band gap like their alkali metal counterparts. Unlike the other cubic sulfides, however, $TlGaSnS_4-cP84$ has an indirect band gap and $TlGaGeSe_4-oP56$ is the only layered orthorhombic compound with an indirect compound. These changes arise likely from the influence of the $Tl-6s$ lone pair states on the electronic structure of the compound. All experimental band gap values and the type of band gap can also be found in Table 4.

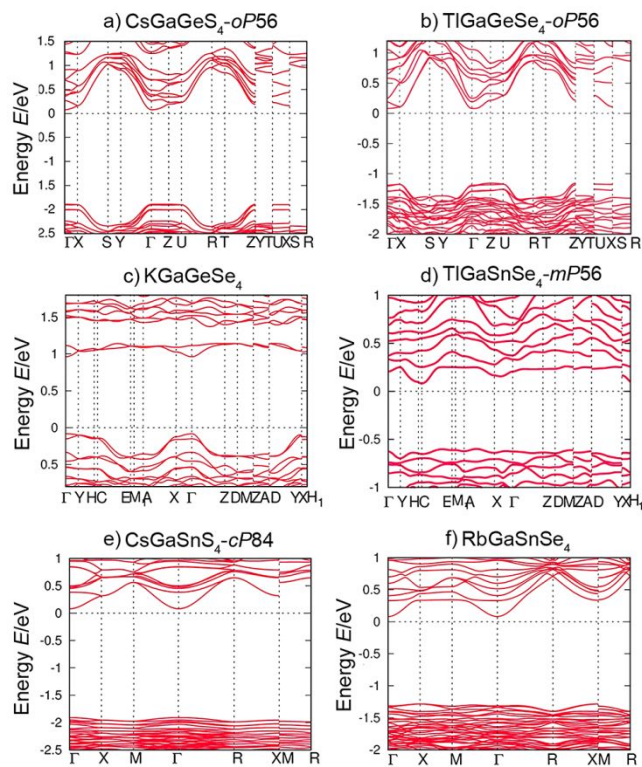


Figure 6. Band structure plots of CsGaGeS₄-oP56 (a), TlGaGeSe₄-oP56 (b), KGaGeSe₄ (c), TlGaSnSe₄-mP56 (d), CsGaSnS₄-cP84 (e), and RbGaSnSe₄ (f), representing the most prominent structures.

Third-Harmonic Generation. For the measurements of the PM behaviors of our new and previously reported $AGaM'Q_4$ compounds, we first investigated the THG counts as a function of particle size (Figures S20). For all $AGaM'Q_4$ compounds, six different particle sizes in the range from 25 – 150 μm were prepared by mechanical sieving of the finely grounded powders. Each material exhibited a THG signal at the smallest particle size (25 – 32 μm). With increasing particle size, a decrease in the THG response was detected, indicating that all materials are non-PM at 1800 nm and 2400 nm (Figure 7, Table 4). Non-PM materials are characterized by a maximum response when the particle size is close to the average coherence length of the compound and a decrease in intensity is observed as the particle size increases.⁶⁸ Consequently, the THG coherence lengths, l_c , for the $AGaM'Q_4$ compounds are assumed to be in the range of 25-32 μm or less. This non-PM behavior is well predicted because of the significant phase mismatch between the fundamental and the THG wavelengths,⁶⁹ which also makes the experimental coherence lengths inaccessible.

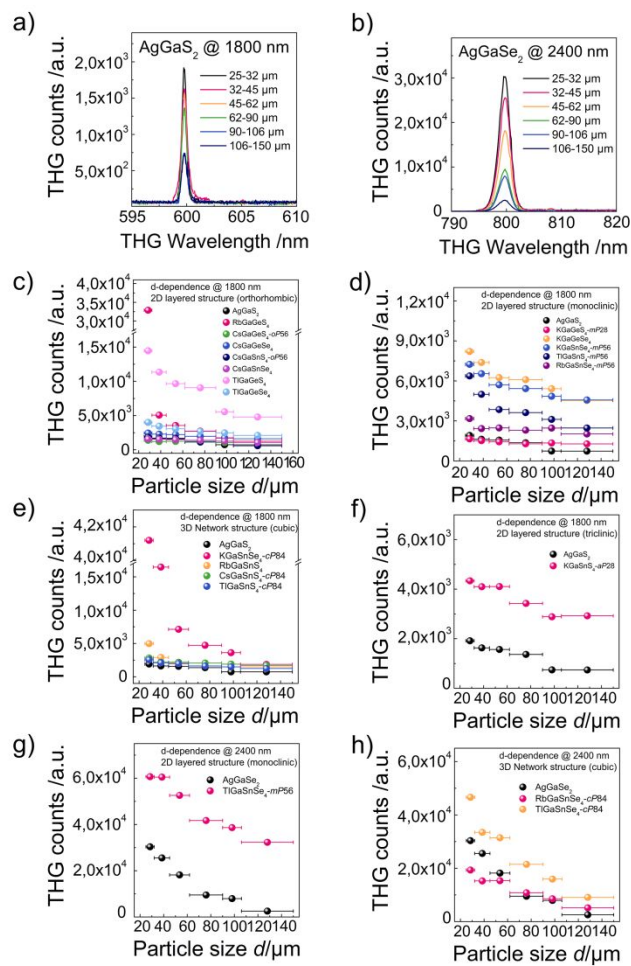


Figure 7. THG spectra of the reference materials AgGaS₂ (a) and AgGaSe₂ (b) for various particle sizes, as well as the corresponding particle size dependence of the various $AGaM'Q_4$ compounds (c-h).

Table 4. Optical band gaps and third-order nonlinear susceptibility values $\chi^{(3)}$ of all the investigated $AGaM'Q_4$ compounds (grain size 25 – 32 μm) sorted by the structure type including the reference material used.

Compound	E_g /eV	THG-Ref.	$\chi^{(3)} \cdot 10^5$ /pm ² V ⁻²
KGaSnSe ₄ -cP84 (14)	2.10 ⁽ⁱ⁾	AgGaS ₂	1.85
RbGaSnS ₄	2.98 ^(d)	AgGaS ₂	0.64
CsGaSnS ₄ -cP84 (18)	3.00 ^(d)	AgGaS ₂	0.48
TlGaSnS ₄ -cP84 (16)	2.50 ⁽ⁱ⁾	AgGaS ₂	0.46
TlGaSnSe ₄ -cP84 (17)	1.84 ⁽ⁱ⁾	AgGaSe ₂	1.98
RbGaSnSe ₄ -cP84 (15)	1.88 ⁽ⁱ⁾	AgGaSe ₂	1.28
RbGaGeS ₄ (1)	3.26 ^(d)	AgGaS ₂	1.66

CsGaGeS ₄ -oP56 (5)	3.18 ^(d)	AgGaS ₂	0.34
CsGaGeSe ₄ (6)	2.14 ^(d)	AgGaS ₂	0.45
CsGaSnS ₄ -oP56 (7)	3.07 ^(d)	AgGaS ₂	0.39
CsGaSnSe ₄	1.97 ^(d)	AgGaS ₂	0.36
TlGaGeS ₄ (3)	2.71 ^(d)	AgGaS ₂	1.10
TlGaGeSe ₄ -oP56 (4)	2.21 ⁽ⁱ⁾	AgGaS ₂	0.58
KGaGeSe ₄ (8)	2.32 ^(d)	AgGaS ₂	0.83
KGaSnSe ₄ -mP56	1.73 ^(d)	AgGaS ₂	0.78
RbGaSnSe ₄ -mP56	2.60 ^(d)	AgGaS ₂	0.51
TlGaSnS ₄ -mP56 (9)	2.49 ⁽ⁱ⁾	AgGaS ₂	0.73
TlGaSnSe ₄ -mP56 (10)	1.95 ⁽ⁱ⁾	AgGaSe ₂	2.26
KGaGeS ₄ -mP28	3.56 ^(d)	AgGaS ₂	0.38
KGaSnS ₄ -aP28	2.60 ^(d)	AgGaS ₂	0.60

*^(d) and ⁽ⁱ⁾ represent direct and indirect band gaps, respectively.

The values for the third-order nonlinear susceptibility $\chi^{(3)}$ of the $AGaM'Q_4$ compounds can be compared with those of $AgGaQ_2$ ($Q = S, Se$) by simply assuming that the coherence lengths of both sample and reference are identical. Using the Kurtz powder method,⁶⁹⁻⁷² the $\chi^{(3)}$ value for each sample was calculated for the non-PM case from the experimentally measured THG counts (I^{THG}) of the sample and the reference by using equation (1).

$$\chi_{Sample}^{(3)} = \chi_{Reference}^{(3)} \left(\frac{I_{Sample}^{THG}}{I_{Reference}^{THG}} \right)^{1/2} \quad (1)$$

Table 4 lists the $\chi^{(3)}$ values calculated at the smallest particle size (25 - 32 μm) of $AgGaQ_2$ and the $AGaM'Q_4$ compounds using $\chi_{Reference}^{(3)} \approx 0.40 \cdot 10^5 \text{ pm}^2 V^{-2}$ for $AgGaS_2$, and $\chi_{Reference}^{(3)} \approx 1.60 \cdot 10^5 \text{ pm}^2 V^{-2}$ for $AgGaSe_2$, respectively.

In general, our measurements indicate that the $AGaM'Q_4$ compounds are excellent candidate materials for THG and other $\chi^{(3)}$ -related applications involving optical switching, self-phase modulation, and four-wave mixing. Most of the investigated compounds exhibit THG responses on par or slightly better than the reference materials $AgGaS_2$ and $AgGaSe_2$, two well-known benchmark materials for NLO applications. More specifically, $TlGaSnSe_4$ -mP56, $TlGaSnSe_4$ -cP84, and $KGaSnSe_4$ -cP84 are most notable because these three selenides outperform the benchmark $AgGaSe_2$. The $AGaM'Q_4$ materials have a higher THG response than $K_4GeP_4Se_{12}$ ²³ or Li_2CdGeS_4 ,⁷² and are on par or slightly below the one-dimensional compounds $K_{(1-x)}Cs_xPSe_6$ and

$CsPSe_6$,²⁴ but lack their SHG properties. These crystalline bulk materials, however, are outclassed by chalcogenide-based glasses and thin films.⁷³⁻⁷⁸

Figure 8a shows the values $\chi^{(3)}$ of all $AGaM'Q_4$ samples sorted by crystal structure and Figure 8b plots those values against the band gap, E_g . At first glance, it seems that most cubic compounds have a higher THG response compared to the lower symmetry solids. However, there appears to be a trend for the $\chi^{(3)}$ as a function of the band gap rather than the crystal structure. The nonlinearity inversely scales with the band gap following a power-law behavior.⁷⁹ In other words, the smaller the band gap the larger the nonlinearity.⁷² However, it should be noted that the wide-gap semiconductor $RbGaGeS_4$ is an outlier to this trend as it exhibits both a large nonlinearity and a large band gap at the same time. This compound is especially promising for high-efficiency/high-power nonlinear applications as it has a larger laser-induced damage threshold owing to its wide-gap nature and is air- and moisture stable.

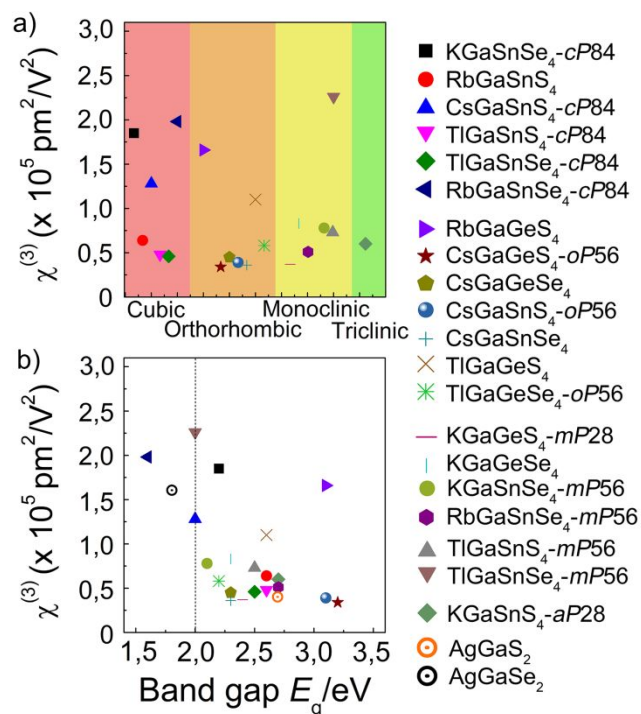


Figure 8. Plots of the third-order nonlinear susceptibility $\chi^{(3)}$ versus (a) the crystal structure and (b) the band gap of the $AGaM'Q_4$ compounds.

Conclusion

Eighteen new quaternary compounds $AGaM'Q_4$ ($A = K, Rb, Cs, Tl; M' = Ge, Sn; Q = S, Se$) were prepared using solid-state syntheses and structurally characterized. This series of compounds constitute the hitherto missing heavier alkali metal $AGaM'Q_4$ compounds in this family. A thorough structural analysis of these and related quaternary phases revealed several cases of

polymorphism for almost all different compositions. Consequently applying these results, new polymorphic modifications of already known compositions could also be isolated and characterized. Furthermore, the mixed M^{3+} and M^{4+} cations in the layered structures both occupy the same cation sites, however, there appears to be some preferred occupation on certain sites especially with a larger difference of the ionic radii of the cations involved. The fact that some polymorphs could not be reproduced shows that the thermodynamic and kinetic parameters leading to the formation of each phase are not fully understood yet and these phases might only form in very specific temperature regions under specific conditions. All chalcogenides are semiconductors with the sulfides having larger band gaps in the blue-UV region compared to the selenides, which can absorb IR-green light. Especially the layered alkali metal compounds $AGaM'Q_4$ ($A = K, Rb, Cs$) with direct band gaps in the UV and Vis region, depending on the composition, are promising candidate materials for optoelectronic applications. THG measurements of this series of chalcogenides revealed a trend of increasing nonlinearity with a decrease of the band gap with a minor dependence on the crystal structure. $RbGaGeS_4$ is the compound with one of the highest THG responses interestingly goes against this trend and exhibits both a large nonlinearity and a large direct band gap, while also not showing any significant irradiation damage. In general, the relatively large nonlinearity of the $AGaM'Q_4$ compounds and the fact that the sulfides are stable under ambient conditions and show no significant irradiation damage make them excellent candidate materials for THG- and other related applications.

ASSOCIATED CONTENT

Supporting Information. Details on the synthesis of compounds 1-18, experimental and theoretical X-ray powder diffraction patterns for the prepared compounds, details on the single X-ray data collection and refinement, atomic coordinates, displacement parameters, and selected interatomic distances for compounds 1-18, band structure and DOS plots for the compounds, and THG spectra of the reference materials and all investigated quaternary compounds. This material is available free of charge via the Internet at <http://pubs.acs.org>.

AUTHOR INFORMATION

Corresponding Author

*E-mail: m-kanatzidis@northwestern.edu

ORCID

Daniel Friedrich: 0000-0001-6953-8114

Shiqiang Hao: 0000-0002-7985-4468

Chris Wolverton: 0000-0003-2248-474X

Joon I. Jang: 0000-0002-1608-8321

Mercouri G. Kanatzidis: 0000-0003-2037-4168

Author Contributions

The manuscript was written through contributions of all authors. All authors have given approval to the final version of the manuscript.

Funding Sources

This work was supported mainly by the National Science Foundation Grant DMR- 2003476. The NLO work was partially supported by an Air Force Office of Scientific Research grant FA9550-19-1-0243. Prof. J.I.J acknowledges support by the Basic Research Program (NRF-2017R1D1A1B03035539 and 2020R1F1A1069646) through the NRF of Korea funded by the Korean government. Dr. Daniel Friedrich would like to thank the German Research Foundation (DFG) for financial support (reference number: FR 4094/1-1). H.R.B. acknowledges support by the National Research foundation of Korea (NRF) grant funded by the Korean government (NRF-2019R1I1A1A01061306).

REFERENCES

- Xiao, C.; Hassanzadeh Fard, Z.; Sarma, D.; Song, T.-B.; Xu, C.; Kanatzidis, M. G. Highly Efficient Separation of Trivalent Minor Actinides by a Layered Metal Sulfide ($KInSn_2S_6$) from Acidic Radioactive Waste. *J. Am. Chem. Soc.* **2017**, 139 (46), 16494-16497.
- Mei, D.; Yin, W.; Feng, K.; Lin, Z.; Bai, L.; Yao, J.; Wu, Y. $LiGaGe_2Se_6$: A New IR Nonlinear Optical Material with Low Melting Point. *Inorg. Chem.* **2012**, 51 (2), 1035-1040.
- Kim, Y.; Seo, I.-s.; Martin, S. W.; Baek, J.; Shiv Halasyamani, P.; Arumugam, N.; Steinfink, H. Characterization of New Infrared Nonlinear Optical Material with High Laser Damage Threshold, $Li_2Ga_2GeS_6$. *Chem. Mater.* **2008**, 20 (19), 6048-6052.
- Yelisseyev, A. P.; Isaenko, L. I.; Krinitsin, P.; Liang, F.; Golosumova, A. A.; Naumov, D. Y.; Lin, Z. Crystal Growth, Structure, and Optical Properties of $LiGaGe_2Se_6$. *Inorg. Chem.* **2016**, 55 (17), 8672-8680.
- Mei, D.; Zhang, S.; Liang, F.; Zhao, S.; Jiang, J.; Zhong, J.; Lin, Z.; Wu, Y. $LiGaGe_2S_6$: A Chalcogenide with Good Infrared Nonlinear Optical Performance and Low Melting Point. *Inorg. Chem.* **2017**, 56 (21), 13267-13273.
- Li, S.-F.; Liu, B.-W.; Zhang, M.-J.; Fan, Y.-H.; Zeng, H.-Y.; Guo, G.-C. Syntheses, Structures, and Nonlinear Optical Properties of Two Sulfides $Na_2In_2MS_6$ ($M = Si, Ge$). *Inorg. Chem.* **2016**, 55 (4), 1480-1485.
- Yin, W.; Feng, K.; Hao, W.; Yao, J.; Wu, Y. Synthesis, Structure, and Properties of $Li_2In_2MQ_6$ ($M = Si, Ge; Q = S, Se$): A New Series of IR Nonlinear Optical Materials. *Inorg. Chem.* **2012**, 51 (10), 5839-5843.
- Yohannan, J. P.; Vidyasagar, K. Syntheses and structural characterization of non-centrosymmetric $Na_2M_2M'S_6$ ($M, M' = Ga, In, Si, Ge, Sn, Zn, Cd$) sulfides. *J. Solid State Chem.* **2016**, 238, 147-155.
- Zhou, M.; Li, C.; Li, X.; Yao, J.; Wu, Y. $K_2Sn_2ZnSe_6$, $Na_2Ge_2ZnSe_6$, and $Na_2In_2GeSe_6$: a new series of quaternary selenides with intriguing structural diversity and nonlinear optical properties. *Dalton Trans.* **2016**, 45 (18), 7627-7633.
- Vu, T. V.; Lavrentyev, A. A.; Gabrelian, B. V.; Tong, H. D.; Parasyuk, O. V.; Khyzhun, O. Y. Electronic band structure and basic optical constants of $TlGaSn_2Se_6$, a promising NLO semiconductor: First-principles calculations under DFT framework. *Optik* **2019**, 181, 673-685.

11. Vu, T. V.; Lavrentyev, A. A.; Gabrelian, B. V.; Parasyuk, O. V.; Khyzhun, O. Y. TlInGe₂S₆, A Prospective Nonlinear Optical Material: First-Principles DFT Calculations of the Electronic Structure and Optical Properties. *J. Electron. Mater.* **2018**, *47* (9), 5525-5536.
12. Vu, T. V.; Lavrentyev, A. A.; Gabrelian, B. V.; Parasyuk, O. V.; Khyzhun, O. Y. First-principles DFT calculations of the electronic structure and optical properties of TlInGe₂Se₆, a prospective NLO material. *Mat. Chem. Phys.* **2018**, *219*, 162-174.
13. Parasyuk, O. V.; Babizhetskyy, V. S.; Khyzhun, O. Y.; Levytskyy, V. O.; Kityk, I. V.; Myronchuk, G. L.; Tsisar, O. V.; Piskach, L. V.; Jedryka, J.; Maciag, A.; Piasecki, M. Novel Quaternary TlGaSn₂Se₆ Single Crystal as Promising Material for Laser Operated Infrared Nonlinear Optical Modulators. *Crystals* **2017**, *7* (11), 341.
14. Yohannan, J. P.; Vidyasagar, K. Syntheses, structural variants and characterization of AInM'S₄ (A = alkali metals, Tl; M' = Ge, Sn) compounds; facile ion-exchange reactions of layered NaInSn₄ and KInSn₄ compounds. *J. Solid State Chem.* **2016**, *238*, 291-302.
15. Al-Bloushi, M.; Davaasuren, B.; Emwas, A.-H.; Rothenberger, A. Synthesis and Characterization of the Quaternary Thioaluminogermanates A(AlS₂)(GeS₂) (A = Na, K). *Z. Anorg. Allg. Chem.* **2015**, *641* (7), 1352-1356.
16. Ward, M. D.; Pozzi, E. A.; Van Duyne, R. P.; Ibers, J. A. Syntheses, structures, and optical properties of the indium/germanium selenides Cs₄In₈GeSe₁₆, CsInSe₂, and CsInGeSe₄. *J. Solid State Chem.* **2014**, *212*, 191-196.
17. Kumari, A.; Vidyasagar, K. Solid-state synthesis, structural variants and transformation of three-dimensional sulfides, AGaSn₄ (A = Na, K, Rb, Cs, Tl) and Na_{1.263}Ga_{1.263}Sn_{0.737}S₄. *J. Solid State Chem.* **2007**, *180* (7), 2013-2019.
18. Hwang, S.-J.; Iyer, R. G.; Trikalitis, P. N.; Ogden, A. G.; Kanatzidis, M. G. Cooling of Melts: Kinetic Stabilization and Polymorphic Transitions in the KInSnSe₄ System. *Inorg. Chem.* **2004**, *43* (7), 2237-2239.
19. Hwang, S.-J.; Iyer, R. G.; Kanatzidis, M. G. Quaternary selenostannates Na_{2-x}Ga_{2-x}Sn_{1+x}Se₆ and AGaSnSe₄ (A = K, Rb, and Cs) through rapid cooling of melts. Kinetics versus thermodynamics in the polymorphism of AGaSnSe₄. *J. Solid State Chem.* **2004**, *177* (10), 3640-3649.
20. Wu, P.; Lu, Y.-J.; Ibers, J. A. Synthesis and structures of the quaternary sulfides KGaSn₄, KInGe₄, and KGaGe₄. *J. Solid State Chem.* **1992**, *97* (2), 383-390.
21. Yuji, N.; Atsushi, A.; Izumi, N.; Kozo, N. The Crystal Structure of a New Thiosilicate of Thallium, TlInSiS₄. *Bull. Chem. Soc. Jpn.* **1984**, *57* (7), 1718-1722.
22. Nakamura, Y.; Nagashima, K.; Nakai, I. Preparation and characterization of the new quaternary chalcogenides Tl-III-IV-S₄ (III = Al, Ga, In; IV = Si, Ge). *Mater. Res. Bull.* **1984**, *19*, 563-570.
23. Jang, J. I.; Park, S.; Harrison, C. M.; Clark, D. J.; Morris, C. D.; Chung, I.; Kanatzidis, M. G. K₄GeP₄Se₁₂: a case for phase-change nonlinear optical chalcogenide. *Opt. Lett.* **2013**, *38* (8), 1316-1318.
24. Haynes, A. S.; Saouma, F. O.; Otieno, C. O.; Clark, D. J.; Shoemaker, D. P.; Jang, J. I.; Kanatzidis, M. G. Phase-Change Behavior and Nonlinear Optical Second and Third Harmonic Generation of the One-Dimensional K_(1-x)Cs_xPSe₆ and Metastable β-CsPSe₆. *Chem. Mater.* **2015**, *27* (5), 1837-1846.
25. Boyd, R. W. *Nonlinear optics* 3rd ed.; Academic Press: 2008.
26. Liao, J. H.; Varotsis, C.; Kanatzidis, M. G. Syntheses, structures, and properties of six novel alkali metal tin sulfides: K₂Sn₂S₈, α-Rb₂Sn₂S₈, β-Rb₂Sn₂S₈, K₂Sn₂S₅, Cs₂Sn₂S₆, and Cs₂SnS₁₄. *Inorg. Chem.* **1993**, *32* (11), 2453-2462.
27. Kubelka, P.; Munk, F. Ein Beitrag zur Optik der Farbanstriche. *Z. tech. Phys.* **1931**, *12*, 593-601.
28. Perdew, J. P.; Burke, K.; Ernzerhof, M. Generalized Gradient Approximation Made Simple. *Physical Review Letters* **1996**, *77* (18), 3865-3868.
29. Kresse, G.; Furthmüller, J. Efficient iterative schemes for ab initio total-energy calculations using a plane-wave basis set. *Phys. Rev. B* **1996**, *54* (16), 11169-11186.
30. Liu, Q.-Q.; Liu, X.; Chen, L.; Wu, L.-M. AGaSnS₄ (A = Rb, Cs): Three sulfides and their structure diversity. *J. Solid State Chem.* **2020**, *285*, 121233.
31. Wang, J.; Li, P.; Cai, T.; Yang, D.-D.; Xiong, W.-W. Four two-dimensional ternary selenides based on group 13 and 14 metals: Syntheses, crystal structures, and electrochemical properties. *J. Solid State Chem.* **2018**, *263*, 88-93.
32. Rubenstein, M.; Roland, G. A monoclinic modification of germanium disulfide, GeS₂. *Acta Cryst. B* **1971**, *27* (2), 505-506.
33. Shannon, R. Revised effective ionic radii and systematic studies of interatomic distances in halides and chalcogenides. *Acta Cryst. A* **1976**, *32* (5), 751-767.
34. Eisenmann, B.; Hofmann, A. Crystal structure of hexapotassium di-μ-selenido-bis(diselenidogallate), K₆Ga₂Se₆. *Z. Kristallogr. Cryst. Mater.* **1991**, *197* (1-2), 153-154.
35. Eisenmann, B.; Hofmann, A. Crystal structure of hexapotassium di-μ-thio-bis(dithiogallate), K₆Ga₂S₆. *Z. Kristallogr. Cryst. Mater.* **1991**, *197* (1-2), 155-156.
36. Eisenmann, B.; Hofmann, A. Crystal structure of pentapotassium tetraselenidogallate(III), K₅GaSe₄. *Z. Kristallogr. Cryst. Mater.* **1991**, *197* (1-2), 163-164.
37. Deiseroth, H. J.; Fu-Son, H. R. Cs₆Ga₂Se₆, ein ternäres Selenogallat(III) mit isolierten (Ga₂Se₆)⁶⁻-Ionen. *Z. Naturforsch. B* **1983**, *38*, 181-182.
38. Schmitz, D.; Bronger, W. Die Kristallstruktur von CsGa₂S₂. *Z. Naturforsch. B* **1975**, *30*, 491-493.
39. Eisenmann, B.; Jakowski, M.; Schäfer, H. Die Strukturen von BaGa₂S₄ und BaAl₂S₄. *Mat. Res. Bull.* **1982**, *17* (9), 1169-1175.
40. Do, J.; Kanatzidis, M. G. The One-dimensional Polyselenide Compound CsGaSe₃. *Z. Anorg. Allg. Chem.* **2003**, *629* (4), 621-624.
41. Kumari, A.; Vidyasagar, K. Rubidium thiogallate. *Acta Cryst. E* **2005**, *61* (9), i193-i195.
42. Friedrich, D.; Schlosser, M.; Pfitzner, A. Interconversion of One-Dimensional Thiogallates Cs₂[Ga₂(S₂)_{2-x}S_{2+x}] (x = 0, 1, 2) by Using High-Temperature Decomposition and Polysulfide-Flux Reactions. *Cryst. Growth Des.* **2017**, *17* (9), 4887-4892.
43. Friedrich, D.; Schlosser, M.; Weihrich, R.; Pfitzner, A. Polymorphism of CsGaS₂ - structural characterization of a new two-dimensional polymorph and study of the phase-transition kinetics. *Inorg. Chem. Front.* **2017**, *4* (2), 393-400.
44. Friedrich, D.; Schlosser, M.; Pfitzner, A. Synthesis and Structural Characterization of Cs₂Ga₂Se₅. *Z. Anorg. Allg. Chem.* **2014**, *640* (5), 826-829.
45. Friedrich, D.; Schlosser, M.; Pfitzner, A. Synthesis and Structural Characterization of the layered Selenogallate RbGaSe₂. *Z. Anorg. Allg. Chem.* **2017**, *643* (21), 1589-1592.
46. Friedrich, D.; Schlosser, M.; Pfitzner, A. Synthesis, Crystal Structure, and Physical Properties of Two Polymorphs of CsGaSe₂, and High-Temperature X-ray Diffraction Study of the Phase Transition Kinetics. *Cryst. Growth Des.* **2016**, *16* (7), 3983-3992.
47. Friedrich, D.; Pielhofer, F.; Schlosser, M.; Weihrich, R.; Pfitzner, A. Synthesis, Structural Characterization, and Physical Properties of Cs₂Ga₂S₅, and Redetermination of the Crystal Structure of Cs₂S₆. *Chem. Eur. J* **2015**, *21* (4), 1811-1817.
48. Goodyear, J.; Steigmann, G. A. The crystal structure of a-Ga₂S₃. *Acta Cryst.* **1963**, *16* (10), 946-949.
49. Hahn, H.; Klingler, W. Über die Kristallstrukturen von Ga₂S₃, Ga₂Se₃ und Ga₂Te₃. *Z. Anorg. Chem.* **1949**, *259* (1-4), 135-142.

50. Hahn, H.; Frank, G. Über die Kristallstruktur des GaS. *Z. Anorg. Allg. Chem.* **1955**, 278 (5-6), 340-348.
51. Schubert, v. K.; Dorre, E.; Kluge, M. Zur kristallchemie der B-metalle. 3. kristallstruktur von GaSe und InTe. *Z. Metallkde.* **1955**, 46 (3), 216-224.
52. Tomas, A.; Pardo, M. P.; Guittard, M.; Guymont, M.; Famy, R. Determination des structures des formes α et β de Ga_2S_3 / structural determination of α and β Ga_2S_3 . *Mat. Res. Bull.* **1987**, 22 (11), 1549-1554.
53. Wu, Y.; Nather, C.; Bensch, W. $\text{Cs}_4\text{Ge}_2\text{S}_8$. *Acta Cryst. E* **2003**, 59 (10), i137-i138.
54. Schlirf, J.; Deiseroth, H. J. Crystal structure of hexacesium hexaselenidodigermanate(III), $\text{Cs}_6\text{Ge}_2\text{Se}_6$. *Z. Kristallogr. NCS* **2001**, 216 (1-4), 27-28.
55. Eisenmann, B.; Hansa, J. Crystal structure of tetrapotassium hexaselenodigermanate, $\text{K}_4\text{Ge}_2\text{Se}_6$. *Z. Kristallogr. Cryst. Mater.* **1993**, 203 (1-2), 301-302.
56. Preishuber-Pflügl, H.; Klepp, K. O. Crystal structure of tetrarubidium hexathiodigermanate(IV), $\text{Rb}_4\text{Ge}_2\text{S}_6$. *Z. Kristallogr. NCS* **2003**, 218 (4), 387-388.
57. Eisenmann, B.; Kieselbach, E.; Schäfer, H.; Schrod, H. Über Thio-, Selenido- und Telluridogermanate (III): Zur Kenntnis von $\text{K}_6\text{Ge}_2\text{S}_6$, $\text{K}_6\text{Ge}_2\text{Se}_6$ und $\text{Na}_6\text{Ge}_2\text{Te}_6$. *Z. Anorg. Allg. Chem.* **1984**, 516 (9), 49-54.
58. Zachariasen, W. H. The Crystal Structure of Germanium Disulphide. *J. Chem. Phys.* **1936**, 4 (9), 618-619.
59. Sheldrick, W. S.; Braunbeck, H.-G. Darstellung und Kristallstruktur von $\text{Rb}_2\text{Sn}_2\text{Se}_5$, ein Rubidium - Selenostannat(IV) mit Raumnetzstruktur/Preparation and Crystal Structure of $\text{Rb}_2\text{Sn}_2\text{Se}_5$, a Rubidium Selenostannate(IV) with Framework Structure. *Z. Naturforsch. B* **1992**, 47 (1), 151-153.
60. Klepp, K. O. Darstellung und Kristallstruktur von $\text{K}_2\text{Sn}_2\text{S}_5$ und $\text{K}_2\text{Sn}_2\text{Se}_5$ / Preparation and Crystal Structure of $\text{K}_2\text{Sn}_2\text{S}_5$ and $\text{K}_2\text{Sn}_2\text{Se}_5$. *Z. Naturforsch. B* **1992**, 47 (2), 197-200.
61. Sheldrick, W. S. Das kantenverknüpfte tritetraedrische Selenostannat(IV)-Anion $[\text{Sn}_3\text{Se}_8]^{4-}$. Darstellung und Struktur von $\text{K}_4\text{Sn}_3\text{Se}_8$ / The Edge-bridged Tritetrahedral Selenostannate(IV) Anion $[\text{Sn}_3\text{Se}_8]^{4-}$. Preparation and Structure of $\text{K}_4\text{Sn}_3\text{Se}_8$. *Z. Naturforsch. B* **1988**, 43 (3), 249-252.
62. Loose, A.; Sheldrick, W. S. Solventothermal Synthesis of the Lamellar Selenostannates(IV) $\text{A}_2\text{Sn}_4\text{Se}_9 \cdot \text{H}_2\text{O}$ (A = Rb, Cs) and $\text{Cs}_2\text{Sn}_2\text{Se}_6$. *Z. Naturforsch. B* **1998**, 53 (3), 349-354.
63. Klepp, K. O.; Fabian, F. $\text{K}_2\text{Sn}_4\text{Se}_8$ - ein gemischtvalentes Selenostannat / $\text{K}_2\text{Sn}_4\text{Se}_8$ - A Mixed-Valent Selenostannate. *Z. Naturforsch. B* **1992**, 47 (3), 406-410.
64. Sheldrick, W. S.; Braunbeck, H. G. Notizen: Darstellung und Kristallstruktur von $\text{Cs}_4\text{Sn}_2\text{Se}_6$ / Preparation and Crystal Structure of $\text{Cs}_4\text{Sn}_2\text{Se}_6$. *Z. Naturforsch. B* **1989**, 44 (7), 851-852.
65. Sheldrick, W. S.; Schaaf, B. Darstellung und Kristallstruktur von $\text{Rb}_2\text{Sn}_3\text{S}_7 \cdot 2 \text{H}_2\text{O}$ und $\text{Rb}_4\text{Sn}_2\text{Se}_6$. *Z. Anorg. Allg. Chem.* **1994**, 620 (6), 1041-1045.
66. Liao, J. H.; Varotsis, C.; Kanatzidis, M. G. Syntheses, structures, and properties of six novel alkali metal tin sulfides: $\text{K}_2\text{Sn}_2\text{S}_8$, α - $\text{Rb}_2\text{Sn}_2\text{S}_8$, β - $\text{Rb}_2\text{Sn}_2\text{S}_8$, $\text{K}_2\text{Sn}_2\text{S}_5$, $\text{Cs}_2\text{Sn}_2\text{S}_6$, and $\text{Cs}_2\text{Sn}_2\text{S}_4$. *Inorganic Chemistry* **1993**, 32 (11), 2453-2462.
67. Okazaki, A.; Ueda, I. The Crystal Structure of Stannous Selenide SnSe . *J. Phys. Chem. Soc. Jpn.* **1956**, 11 (4), 470.
68. Kurtz, S. K.; Perry, T. T. A Powder Technique for the Evaluation of Nonlinear Optical Materials. *J. Appl. Phys.* **1968**, 39 (8), 3798-3813.
69. Brant, J. A.; Clark, D. J.; Kim, Y. S.; Jang, J. I.; Weiland, A.; Aitken, J. A. Outstanding Laser Damage Threshold in $\text{Li}_2\text{MnGeS}_4$ and Tunable Optical Nonlinearity in Diamond-Like Semiconductors. *Inorg. Chem.* **2015**, 54 (6), 2809-2819.
70. <http://marzenell.de/Research/Z-Scan/z-scan.html>
71. Li, W.; Li, Y.; Xu, Y.; Lu, J.; Wang, P.; Du, J.; Leng, Y. Measurements of nonlinear refraction in the mid-infrared materials ZnGeP_2 and AgGaS_2 . *Appl. Phys. B* **2017**, 123 (3), 82.
72. Jang, J. I.; Clark, D. J.; Brant, J. A.; Aitken, J. A.; Kim, Y. S. Highly efficient infrared optical nonlinearity of a wide-bandgap chalcogenide $\text{Li}_2\text{CdGeS}_4$. *Opt. Lett.* **2014**, 39 (15), 4579-4582.
73. Rani, S.; Mohan, D.; Kumar, M.; Sanjay. Study of third order nonlinearity of chalcogenide thin films using third harmonic generation measurements. *Opt. Mater* **2018**, 79, 220-222.
74. Hou, Y.; Liu, Q.; Zhou, H.; Gao, C.; Qian, S.; Zhao, X. Ultrafast non-resonant third-order optical nonlinearity of GeS_2 - Ga_2S_3 - CdS chalcogenide glass. *Solid State Commun.* **2010**, 150 (17), 875-878.
75. Zhang, X.-Y.; Chen, F.-F.; Zhang, X.-H.; Ji, W. Research progress of third-order optical nonlinearity of chalcogenide glasses. *Chin. Phys. B* **2018**, 27 (8), 084208.
76. Kohoutek, T.; Mizuno, S.; Suzuki, T.; Ohishi, Y.; Matsumoto, M.; Misumi, T. Third-harmonic generation measurement of nonlinear optical susceptibility $\chi^{(3)}$ of Ge-Ga-Sb-S chalcogenide glasses proposed for highly nonlinear photonic fibers. *J. Opt. Soc. Am. B* **2011**, 28 (2), 298-305.
77. Kanbara, H.; Fujiwara, S.; Tanaka, K.; Nasu, H.; Hirao, K. Third-order nonlinear optical properties of chalcogenide glasses. *Appl. Phys. Lett.* **1997**, 70 (8), 925-927.
78. Zhou, Z. H.; Hashimoto, T.; Nasu, H.; Kamiya, K. Two-photon absorption and nonlinear refraction of lanthanum sulfide-gallium sulfide glasses. *J. Appl. Phys.* **1998**, 84 (5), 2380-2384.
79. Jackson, A. G.; Ohmer, M. C.; LeClair, S. R. Relationship of the second order nonlinear optical coefficient to energy gap in inorganic non-centrosymmetric crystals. *Infrared Physics & Technology* **1997**, 38 (4), 233-244.

TOC Graphic

